Mapping gaseous amines, ammonia, and their particulate counterparts in marine atmospheres of China's marginal seas: Part 2 - spatiotemporal heterogeneity, causes, and hypothesis

Yating Gao[1], Dihui Chen[1], Yanjie Shen[1], Yang Gao[1,2], Huiwang Gao[1,2], Xiaohong Yao[1,2*]

[1]Key Laboratory of Marine Environment and Ecology, and Frontiers Science Center for Deep Ocean Multispheres and Earth System, Ministry of Education, Ocean University of China, Qingdao 266100, China

[2]Laboratory for Marine Ecology and Environmental Science, Qingdao National Laboratory for Marine Science and Technology, Qingdao 266237, China

*Correspondence to: Xiaohong Yao (xhyao@ouc.edu.cn)

Abstract. Spatiotemporal heterogeneities in the concentrations of alkaline gases and their particulate counterparts in the marine atmosphere over China's marginal seas were investigated in terms of causes and chemical conversion during two winter cruise campaigns, using semi-continuous measurements made by an onboard URG-9000D Ambient Ion Monitor-Ion chromatograph (AIM-IC, Thermo Fisher). During the cruise campaign over the East China Sea from December 27, 2019 to January 6, 2020, the concentrations of gas phase atmospheric trimethylamine (TMA_{gas}) varied by approximately one order of magnitude, with an average ($\pm$ standard deviation) of 0.10 ± 0.04 µg m^{-3} corresponding to mixing ratio of 26 ± 17 pptv. Corresponding mean values were 0.037 ± 0.011 µg m^{-3} (14 ± 5 pptv in mixing ratio) over the Yellow Sea during the period from 7 to 16 January 2020 and 0.031 ± 0.009 µg m^{-3} (12 ± 4 pptv in mixing ratio) over the Yellow Sea and the Bohai Sea from 9 to 22 December 2019. By contrast, the simultaneously observed concentrations of TMA in $PM_{2.5}$, detected as $TMAH^+$, over the East China Sea were 0.098 ± 0.068 µg m^{-3} and substantially smaller than the 0.28 ± 0.18 µg m^{-3} observed over the Yellow Sea and the Bohai Sea from 9 to 22 December 2019. A significant correlation between TMA_{gas} and particulate $TMAH^+$ was observed over the East China Sea, but no correlation was found over the Yellow Sea and Bohai Sea. Proportional or disproportional variations in concentrations of TMA_{gas} with particulate $TMAH^+$ over the sea zones were probably attributed to the difference in the enrichment of $TMAH^+$ in the sea surface microlayer. In addition, spatiotemporal heterogeneities in concentrations of

atmospheric ammonia (NH_{3gas}), atmospheric dimethylamine (DMA_{gas}), and DMA in $PM_{2.5}$, detected as $DMAH^+$, were investigated. Case analyses were performed to illustrate the formation and chemical conversion of particulate aminium ions in marine aerosols. Finally, we hypothesized the release of basic gases and particulate counterparts from the ocean to the atmosphere, together with the secondary formation of $DMAH^+$ and chemical conversion of $TMAH^+$, in the marine atmosphere.

1 Introduction

In the marine atmosphere, gaseous ammonia (NH_{3gas}) and amines, including trimethylamine (TMA_{gas}) and dimethylamine (DMA_{gas}), are unique alkaline gases that play an important role in neutralizing acids (Gibb et al., 1999; Johnson et al., 2007, 2008; Ge et al., 2011; Carpenter et al., 2012; Yu and Luo, 2014; Paulot et al., 2015; Wentworth et al., 2016; Chen et al., 2016; Köllner et al., 2017; van Pinxteren et al., 2019; Perraud et al., 2020). The release of NH_{3gas} from the ocean to the atmosphere is determined mainly by NH_4^+ concentrations in bulk seawater, surface seawater temperature, and pH of surface seawater (Johnson et al., 2007, 2008; Carpenter et al., 2012). Biochemical origins of TMA and DMA in marine atmospheres have been well documented to be released from the degradation of glycine betaine (GBT) and trimethylamine N-oxide (TMAO), which help marine organisms resist the salinity fluctuations (Lidbury et al., 2014, 2015). As organic alkali, TMA and DMA can be dissolved in water as well as liquid organics. In addition to the aforementioned factors, the release of TMA_{gas} and DMA_{gas} from the ocean to the atmosphere may also be affected by the sea surface microlayer (SML), because of the enrichment of TMA and DMA therein (van Pinxteren et al., 2019). In addition, TMA and DMA in bulk seawater theoretically undergo protonation as $TMAH^+$ and $DMAH^+$. However, whether the amines enriched in the SML undergo protonation remains unclear. The differences between inorganic and organic alkali cause different spatiotemporal variations in sea-derived emissions and concentrations of NH_{3gas} from TMA_{gas} and DMA_{gas}, generating a large spatiotemporal heterogeneity in the molar ratios of TMA_{gas} (DMA_{gas}) to NH_{3gas} in various marine atmospheres (Gibb et al., 1999). In exploring spatiotemporal heterogeneity and its causes, high-time-resolution observational data are required.

Two additional factors can also complicate the spatiotemporal heterogeneity of the ratios in marine atmospheres. First, decay of phytoplankton blooms on the surface and subsurface seawater may lead to the accumulation of NH_4^+ therein (Johnson et al., 2007, 2008; Liu et al., 2013). However, NH_4^+ is an important nutrient that can be rapidly reused by phytoplankton in seawater (Velthuis et al., 2017; Zhang et al., 2019a, b). Reuse of aminium ions by phytoplankton is theoretically possible, but according to our review of the literature, has not been investigated. Two scenarios can be hypothesized: a) the reuse of aminium ions by phytoplankton as quickly as that of NH_4^+ and b) slow reuse of aminium ions by phytoplankton. Second, TMA and DMA may further biochemically decompose into small molecules (Hu et al., 2015, 2018; Lidbury et al., 2014, 2015; Xie et al., 2018). These two factors would alter the ratios of TMA_{gas} (DMA_{gas}) to NH_{3gas} in oceanic emissions in opposite directions.

Unlike the release of alkaline gases, the release of primary particulate aminium aerosols from the ocean should be behaviorally similar to that of sea spray organic aerosols and be strongly affected by the SML (Quinn, et al., 2015; Hu et al., 2018; Dall'Osto et al., 2019). In addition to primary emissions, secondary reactions have been reported as important sources of particulate aminium aerosols in marine atmosphere (Facchini et al., 2008; Müller et al., 2009; Xie et al., 2018; Hu et al., 2015, 2018; Köllner et al., 2017; Dall'Osto et al., 2019; Zhou et al., 2019). However, it is challenging to robustly identify primary aminium aerosols from secondary aminium aerosols in the marine atmosphere. Moreover, what remains poorly understood is whether the detected particulate aminium ions by ion chromatography, or particulate amines by mass spectrum, exist in the organic phase, aqueous phase, or mixed phase in the marine atmosphere (Ault et al., 2013; Prather et al., 2013; Pankow, 2015; Xie et al., 2018).

In a companion paper (Chen et al., 2021), we focused on identifying sea-derived alkali gases and particulate counterparts in $PM_{2.5}$ during a winter cruise campaign over the Yellow Sea and Bohai Sea, determined by an onboard URG-9000D Ambient Ion Monitor-Ion chromatograph (AIM-IC, Thermo Fisher). In this study, we focused on investigating the spatiotemporal heterogeneity of concentrations of NH_{3gas}, TMA_{gas}, and DMA_{gas}, together with their particulate counterparts in marine atmospheres, by comparing observations during two winter cruise campaigns over the Yellow Sea, Bohai Sea, and the East China Sea. Moreover, previously reported episodic concentrations of particulate $TMAH^+$ and $DMAH^+$ observed in the marine atmosphere over the Yellow Sea were also included to deepen the

85   understanding of size distributions of aminium ions, the ratio of aminium ions to NH_4^+, and related primary or secondary origins of particulate aminium ions. Building on the analysis results, a hypothesis is presented to illustrate the release of gaseous alkali and their counterparts from the ocean to the atmosphere, and related chemical conversions in the marine atmosphere.

2 Experimental

90   From December 27, 2019 to January 17, 2020, a round cruise survey, focusing on air-sea exchanges of greenhouse gases and short-lived reactive gases was conducted in China over the East China Sea and the Yellow Sea using an R/V Dongfanghong-3. The cruise routes during the campaign and immediately before are shown in Figure S1a, b. The cruise campaigns from 9 to 22 December 2019 and from December 27, 2019 to January 17, 2020, are here referred to as Campaigns A and B, respectively.

95   Details on the measurements during Campaign B were the same as those reported in the companion paper: the onboard AIM-IC was housed in air-conditioned containers and semi-continuously measured the hourly average concentrations of gaseous species of interest and particulate counterparts in $PM_{2.5}$. The limits of detection of NH_4^+, $DMAH^+$, and $TMAH^+$ in the atmosphere were 0.0004, 0.004, and 0.002 µg m^{-3}, respectively. In Campaign B, no K^+ contamination occurred in the channel used to

100   determine gaseous species, and the concentrations of DMA_{gas} and TMA_{gas} could be determined (Fig. 1a). However, strong K^+ contamination unexpectedly occurred in the channel used to determine particulate species from January 7, 2020, leading to no data for $DMAH^+$ and $TMAH^+$ in $PM_{2.5}$ after that date (Fig. 1b). However, concentrations of NH_4^+ and other ions, excluding K^+, were not affected because their residence time in the ion chromatograph was far from that of K^+. Note that mono

105   methylamine cannot be detected by AIM-IC by using the analytical column CS17A (2 x 250 mm) in this study. Concentrations of triethylamine were generally undetectable, therefore, the data were not analyzed here. No biogenic origin in marine environment has been reported for diethylamine, although it may be detected as $TMAH^+$ by AIM-IC. In 2021, we tried a new analytical column CS20 (2 x 250 mm) to analyze amines, including diethylamine, and the unpublished data confirmed its concentration

110   to be negligible relative to $TMAH^+$ in the marine atmosphere of marginal seas of China.

The AIM-IC expectedly encountered terminations several times during Campaign B. This is quite normal for most online analyzers after operating for two weeks on a swaying research vessel, especially when the cruise frequently encounters strong winds. Considering that strong winds substantially increase air-sea exchange fluxes, all instruments were operated to continuously capture the signals.

After restarting the AIM-IC, it always reported a few abnormally high values in the first 3-5 h because of residuals in the system. Abnormal values were excluded from the analysis. Moreover, 24-hour air mass backward trajectories at 100 m, 500 m, and 1000 m above sea level were calculated using the National Oceanic and Atmospheric Administration Air Resources Laboratory's Hybrid Single-Particle Lagrangian Integrated Trajectory model (HYSPLIT; https://ready.arl.noaa.gov/HYSPLIT.php).

In addition, observations made over the Yellow Sea from 2 to 21 May 2012 were included to facilitate analyses. These data were reported in our previous study (Hu et al., 2015), in which the total concentrations of $TMAH^+$ in three size-segregated atmospheric particle samples were also found to reach a high level of ~1 µg m^{-3}. Notably, high concentrations of particulate $TMAH^+$ were not observed in marine atmospheres during additional multiple cruise campaigns from the marginal seas of China to the northwest Pacific Ocean (Xie et al., 2018; Hu et al., 2018; Zhu et al., 2019). In the study reported by Hu et al. (2015), a low-volume Anderson cascade impactor (AN-200; Sibata Co., Inc., Japan) was employed to collect atmospheric particles with 50% aerodynamic cut-off diameters of 11, 7.0, 4.7, 3.3, 2.1, 1.1, 0.65, and 0.43 µm. Details of the sampling and chemical analyses can be found in Hu et al. (2015). The cruise campaign was referred to as Campaign C in this study, and the sea zones collected from the three aerosol samples are shown in Figure S1c.

3 Results and discussion

3.1 Spatiotemporal variations in concentrations of alkaline gases over the East China Sea and the Yellow Sea

Table 1. Information on the three campaigns and concentrations of TMA_{gas} and DMA_{gas} and their particulate partners in $PM_{2.5}$ (average ± standard deviation).

Name	Date	Location	Average concentration (µg m^{-3})			
			$TMAH^+$ in $PM_{2.5}$	$DMAH^+$ in $PM_{2.5}$	TMA_{gas}	DMA_{gas}

Campaign		Date	Location				
Campaign A		Dec. 9 - 22, 2019 (E-period 3, Dec. 15-19)	the Bohai Sea and the Yellow Sea	0.28±0.18 (0.39±0.24)	0.065±0.068 (0.039±0.034)	0.031±0.009 (0.037±0.009)	0.006±0.006 (0.007±0.007)
Campaign B	E-period 1	Dec. 27, 2019 - Jan. 7, 2020	the East China Sea	0.098±0.068	0.019±0.014	0.10±0.04	0.012±0.011
	E-period 2	Jan. 7 - 16, 2020	the Yellow Sea	-	-	0.037±0.011	0.002±0.001
Campaign C		May 2 - 21, 2012	the Yellow Sea	0.43±0.43 (in PM$_{11}$)	0.20±0.17 (in PM$_{11}$)	-	-
Potential dominant sources		-	-	marine	both marine and continental transport	marine	both marine and continental transport

Figure 1a, b shows spatiotemporal variations in concentrations of TMA$_{gas}$, DMA$_{gas}$, and NH$_{3gas}$ and their counterparts in PM$_{2.5}$ during Campaign B (Note that the corresponding mass concentrations of PM$_{2.5}$ were not available in this study), and Table 1 summarizes the observational results during the three campaigns. The corresponding wind speeds and directions are shown in Figure 1c. Some concentrations of TMA$_{gas}$, particulate TMAH$^+$, and wind fields are mapped in Figure 1d-f. Concentrations of TMA$_{gas}$ ranged from 0.022 μg m^{-3} (8 pptv in mixing ratio) to 0.22 μg m^{-3} (91 pptv in mixing ratio) over the East China Sea from December 27, 2019 to January 6, 2020. Corresponding average values were 0.10±0.04 μg m^{-3} (26±17 pptv in mixing ratio).
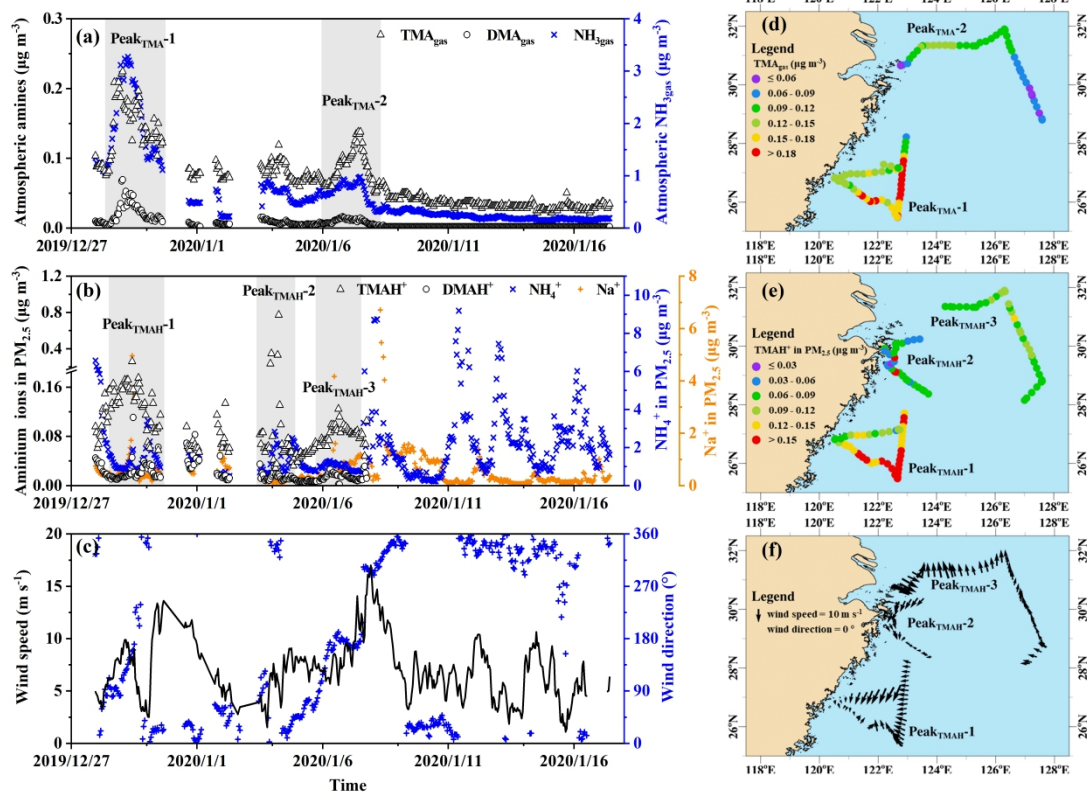
Figure 1: Time series and maps of basic gases and particulate counterparts in concentration and meteorological parameters during the cruise campaign from 27 December 2019 to 17 January 2020: time series of TMA$_{gas}$, DMA$_{gas}$ and NH$_{3gas}$ (a); time series of TMAH$^+$, DMAH$^+$, and NH$_4^+$ in PM$_{2.5}$ (b); time series of wind speed and wind directions (c), map of TMA$_{gas}$ (d); map of TMAH$^+$ (e); map of wind fields (f); not all data were shown in (d-f) to avoid clustering.

The values largely decreased to 0.037±0.011 µg m^{-3} (14±5 pptv in mixing ratio) over the Yellow Sea from 7 to 16 January 2020. The latter concentrations were comparable to those of 0.031±0.009 µg m^{-3} (12±4 pptv in mixing ratio) observed over the Yellow Sea and the Bohai Sea during Campaign A (Chen et al., 2021). Based on the evidence provided as follows, long-range continental transport should be a negligible contributor to the observed TMA$_{gas}$ in the marine atmosphere. Alternatively, the observed TMA$_{gas}$ during the period of Campaign B was probably determined by oceanic emissions of TMA$_{gas}$ from the cruise sea zone.

1) No increase in TMA$_{gas}$ was detected with several periodically large increases in particulate NH$_4^+$ under offshore winds over the Yellow Sea from 7 to 16 January 2020 (Fig. 1a-c). By contrast, higher concentrations of NH$_4^+$ were associated with lower values of TMA$_{gas}$ over the East China Sea and vice

160 versa (Fig. 1a, b; the start period of Campaign B). Higher concentrations of NH_4^+ reflected an increased

contribution from continent input because of insufficient SO_2 and NO_x to form ammonium aerosols.

The calculated 24-hr air mass backward trajectories at 100 m, 500 m, and 1000 m implied that the air

masses were derived from the continental atmosphere (Fig. S4a). Moreover, two broad peaks of

TMA_{gas} were observed over the East China Sea, approximately 200 km from the continent, under

165 onshore winds (Fig. 1d, f). The calculated trajectories implied that the air masses were derived from the

marine atmosphere (Fig. S4b, c, d). Combining the concentrations of TMA_{gas} in the continental

atmosphere upwind of the Yellow Sea with these results allowed us to infer that continental transport

represents a negligible contribution to the observed TMA_{gas} during Campaign B.

2) The concentrations of TMA_{gas} in the continental atmosphere upwind of the Yellow Sea during the

170 summer and fall of 2019 remained at a low level of ~0.002 µg m^{-3} (Chen et al., 2021) and were over

one order of magnitude smaller than the values over the Yellow Sea from 7 to 16 January 2020. An

even larger difference was observed when the observed concentrations of TMA_{gas} over the East China

Sea were compared with continental values. Unfortunately, no recent measurements of TMA_{gas} in the

coastal atmosphere upwind of the East China Sea were available for comparison.

175 3) A moderately good exponential correlation ($TMA_{gas}=0.03 \times e^{0.08T}$; $R^2=0.76$, P<0.01) was observed

between the concentrations of TMA_{gas} and ambient air temperature (Fig. 2a). Although the surface

seawater temperature was not measured, it could reasonably be approximated from the ambient air

temperature (Deng et al., 2014). The exponential correlation suggested that the observed concentrations

of TMA_{gas} were probably determined by the temperature-driven oceanic emission of TMA_{gas} in the

180 corresponding sea zones. Across the same ambient temperature ranges, the observed concentrations of

TMA_{gas} over the East China Sea (full dots in Fig. 2a) were larger than those over the Yellow Sea

(empty dots in Fig. 2a). The regression equation derived was $TMA_{gas}=0.03 \times e^{0.05T}$ ($R^2=0.56$, P<0.01)

when data measured over the Yellow Sea during Campaign B were used alone. We compared the two

derived regression equations and could infer that the temperature-driven oceanic emissions of TMA_{gas}

185 over the East China Sea were larger than those over the Yellow Sea. In addition to temperature, the pH

of surface seawater and the concentration of $TMAH^+$ in surface seawater may also affect TMA_{gas}

emissions (van Pinxteren et al., 2019). Considering approximately constant pH values of 8.0-8.2 in

surface seawater across the two sea zones (Lui et al., 2015; Shao et al., 2020), the concentrations of

TMAH$^+$ in the surface seawater of the East China Sea were expected to be larger than those over the

190 Yellow Sea during Campaign B. Unfortunately, no direct measurements were made to confirm this.

To enlarge the dataset measured over the Yellow Sea, we included the measurements from 15:00LT (local time; UTC+08:00) on December 16 to 01:00LT on December 19 during Campaign A. During this period in Campaign A, concentrations of TMA$_{gas}$ were higher than those observed during other periods in Campaign A at the same ambient air temperature (Chen et al., 2021). We combined the data

195 during this period with data measured over the Yellow Sea during Campaign B to derive the regression equation: TMA$_{gas}$=0.03×e$^{0.05T}$ (Fig. S2), which is the same as that derived from the data measured over the Yellow Sea during Campaign B alone. However, R^2 slightly decreased to 0.54, with P<0.01. This result further supports the lower temperature-driven oceanic emissions of TMA$_{gas}$ from the Yellow Sea.
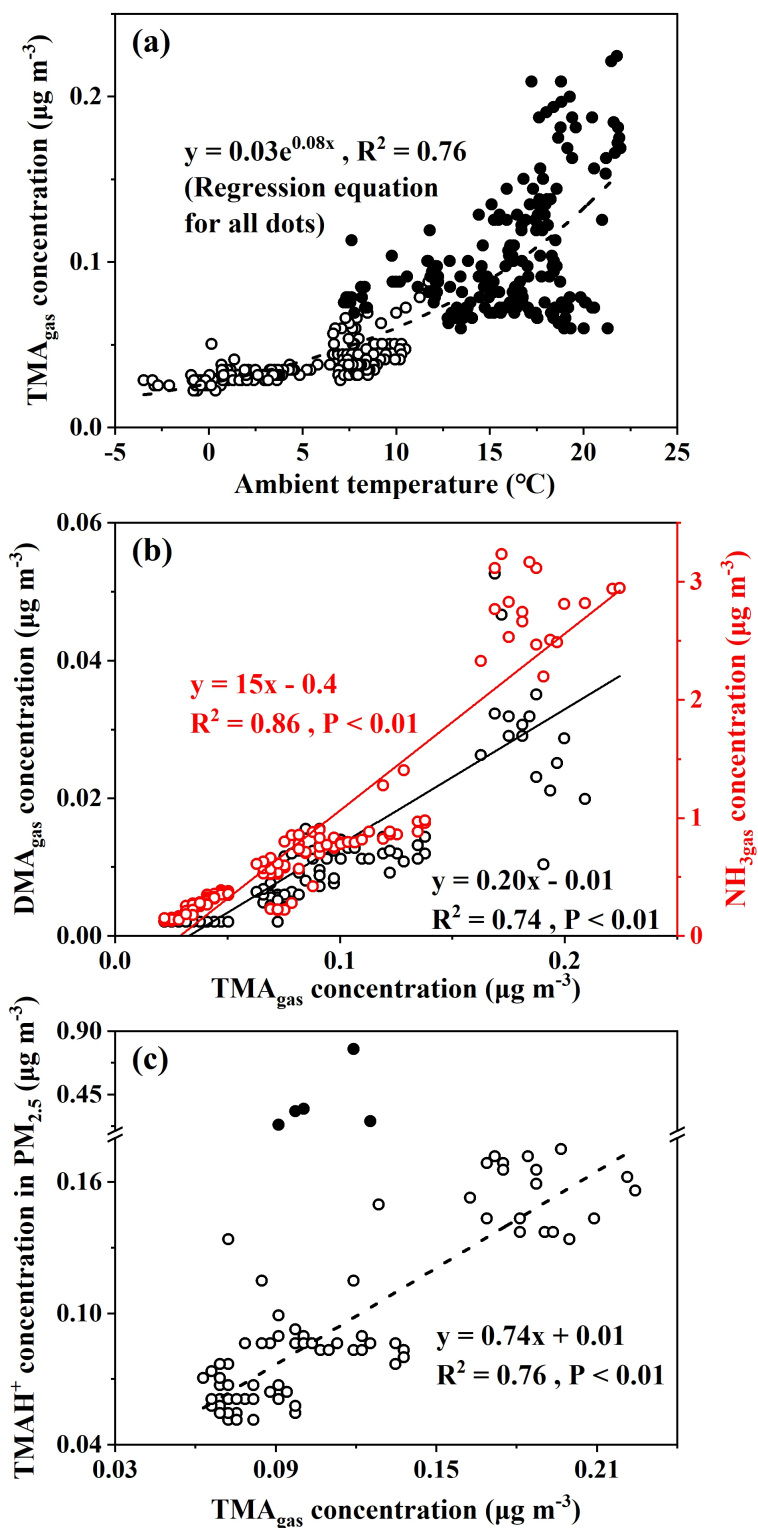
Figure 2: Correlations of TMA_{gas} with ambient air temperature, DMA_{gas}, NH_{3gas}, and $TMAH^+$ in $PM_{2.5}$ with TMA_{gas} (TMA_{gas} vs. ambient air temperature (a); DMA_{gas} and NH_{3gas} vs. TMA_{gas} (b); $TMAH^+$ vs. TMA_{gas} (b); full dots in (b) represent five episodic concentrations of $TMAH^+$ and were excluded for correlation analysis)

Spatiotemporal variations in concentrations of DMA_{gas} and NH_{3gas} were similar to those of TMA_{gas} during Campaign B. For example, concentrations of DMA_{gas} and NH_{3gas} varied 0.012 ± 0.011 μg m^{-3} and 1.1 ± 0.76 μg m^{-3}, respectively, over the East China Sea. However, they largely decreased to 0.002 ± 0.001 μg m^{-3} and 0.24 ± 0.08 μg m^{-3}, respectively, over the Yellow Sea. In addition, concentrations of DMA_{gas} and NH_{3gas} had moderately good and good correlations with those of TMA_{gas} (Fig. 2b), respectively, that is, $DMA_{gas} =0.20 \times [TMA_{gas}]$ -0.01, R^2=0.74, P<0.01, and NH_{3gas} =15×[TMA_{gas}] -0.40, R^2=0.86, and P<0.01. The correlations suggested that the observed DMA_{gas} and NH_{3gas} were also generally derived from marine emissions simultaneously with TMA_{gas}. Thus, we concluded that the seas were the net sources of DMA_{gas} and NH_{3gas} during the study. Note that the residence time of NH_{3gas} is substantially shorter than that of NH_4^+ aerosols (Yao and Zhang, 2013), and less long-range transport of NH_{3gas} was expected than NH_4^+ aerosols. In addition, the observed ratios of TMA_{gas} to NH_{3gas} were two orders of magnitude larger than those that have been reported in marine atmospheres and adopted for modeling (Van Neste, et al., 1987; Gibb et al., 1999; Yu and Luo, 2014). To the best of our knowledge, no recent measurements of TMA_{gas} and NH_{3gas} in a marine atmosphere have been recently reported in the literature. Zheng et al. (2015) measured the concentrations of TMA_{gas} and NH_{3gas} in the continental atmosphere in Nanjing, China. The ratio of TMA_{gas} to NH_{3gas} was approximately 0.4×10^{-3}. However, the observed ratios of DMA_{gas} to NH_{3gas} were reasonably comparable to previously reported values (Yu and Luo, 2014).

3.2 Spatiotemporal variations in concentrations of particulate $TMAH^+$, $DMAH^+$, and NH_4^+ over the East China Sea

Concentrations of $TMAH^+$ in $PM_{2.5}$ varied approximately 0.098 ± 0.068 μg m^{-3} over the East China Sea, but no data could be obtained over the Yellow Sea during the cruise because of K^+ contamination. Almost all values were smaller than 0.2 μg m^{-3}, except five episodic values of 0.26 μg m^{-3} at 10:00LT on 29 December 2019, 0.23 μg m^{-3} and 0.35 μg m^{-3} at 22:00-23:59LT on 3 January and 0.33 μg m^{-3} and 0.77 μg m^{-3} at 05:00-06:59LT on 4 January 2020 (Fig. 1b). Concentrations of $TMAH^+$ exhibited a moderately good correlation with those of TMA_{gas} simultaneously observed over the East China Sea when the five episodes with concentrations of $TMAH^+$ in $PM_{2.5}$ exceeding 0.2 μg m^{-3} were excluded from the correlation (Fig. 2c), suggesting that the $TMAH^+$ in $PM_{2.5}$ may also be derived from marine

sources. In addition, a broad peak of TMAH$^+$ concentrations (Peak$_{TMAH-1}$ shadowing in Fig. 1b) was observed from 27 to 30 December 2019, when a negative correlation existed between the concentrations of TMAH$^+$ and NH$_4$$^+$, with R^2=0.35, and P<0.01. The negative correlation also supported the conclusion that increased concentrations of TMAH$^+$ in PM$_{2.5}$ were driven by enhanced marine emissions rather than continental transport.

The large increases in concentrations of particulate NH$_4$$^+$, for example, when its concentrations exceed 5 µg m^{-3}, under offshore winds, clearly indicated the continental transport of air pollutants (Figs. 1bc, S1a). However, when its concentration was below 1 µg m^{-3}, a significant correlation between particulate NH$_4$$^+$ and TMAH$^+$ was apparent, with P<0.01 (empty dots Fig. 3a). When five points with concentrations of particulate TMAH$^+$ exceeding 0.2 µg m^{-3} were included in the correlation analysis (full dots in Fig. 3a), R^2 increased to 0.62. Thus, primary sea-derived particulate NH$_4$$^+$ could not be excluded from the marine atmosphere over the East China Sea. On the basis of the regression equation shown in Figure 3a, the estimated primary sea-derived particulate NH$_4$$^+$ should be smaller than 0.48 µg m^{-3} under concentrations of particulate TMAH$^+$ below 0.2 µg m^{-3}. Altieri et al. (2014) used isotopic data and identified a marine ammonium source in rainwater in Bermuda, but they did not specify whether marine ammonium was derived from primary particulate emissions.

Concentrations of DMAH$^+$ in PM$_{2.5}$ varied around 0.019±0.014 µg m^{-3} over the East China Sea. The average value was only one-fifth that of TMAH$^+$ in PM$_{2.5}$, but it was almost double that of the DMA$_{gas}$ simultaneously observed. The average value of DMAH$^+$ in PM$_{2.5}$ was also approximately one-third the value observed over the Yellow Sea and the Bohai Sea on 9-22 December (0.065±0.068 µg m^{-3}) (Chen at al., 2021). Positive correlations between DMAH$^+$ and NH$_4$$^+$ were demonstrated, with P<0.01, but the R^2 value was 0.17 (all dots in Fig. 3b). However, when NH$_4$$^+$ concentrations exceeded 5 µg m^{-3}, there was a good correlation between DMAH$^+$ and NH$_4$$^+$ ([DMAH$^+$] = 0.014×[NH$_4$$^+$] - 0.049, R^2=0.80, P<0.01) (full dots in Fig. 3b). When NH$_4$$^+$ concentrations were in the range of 2-4 µg m^{-3} (half full dots in Fig. 3b), a moderately good correlation of DMAH$^+$ existed with NH$_4$$^+$ ([DMAH$^+$] = 0.013×[NH$_4$$^+$] - 0.012, R^2=0.71, P<0.01), when one outlier was omitted. The good and moderately good correlations, together with the negative intercepts in the regression equations, suggested a dominant contribution from continental transport to the observed DMAH$^+$ when NH$_4$$^+$ concentrations exceeded 2 µg m^{-3}, except for the outlier.
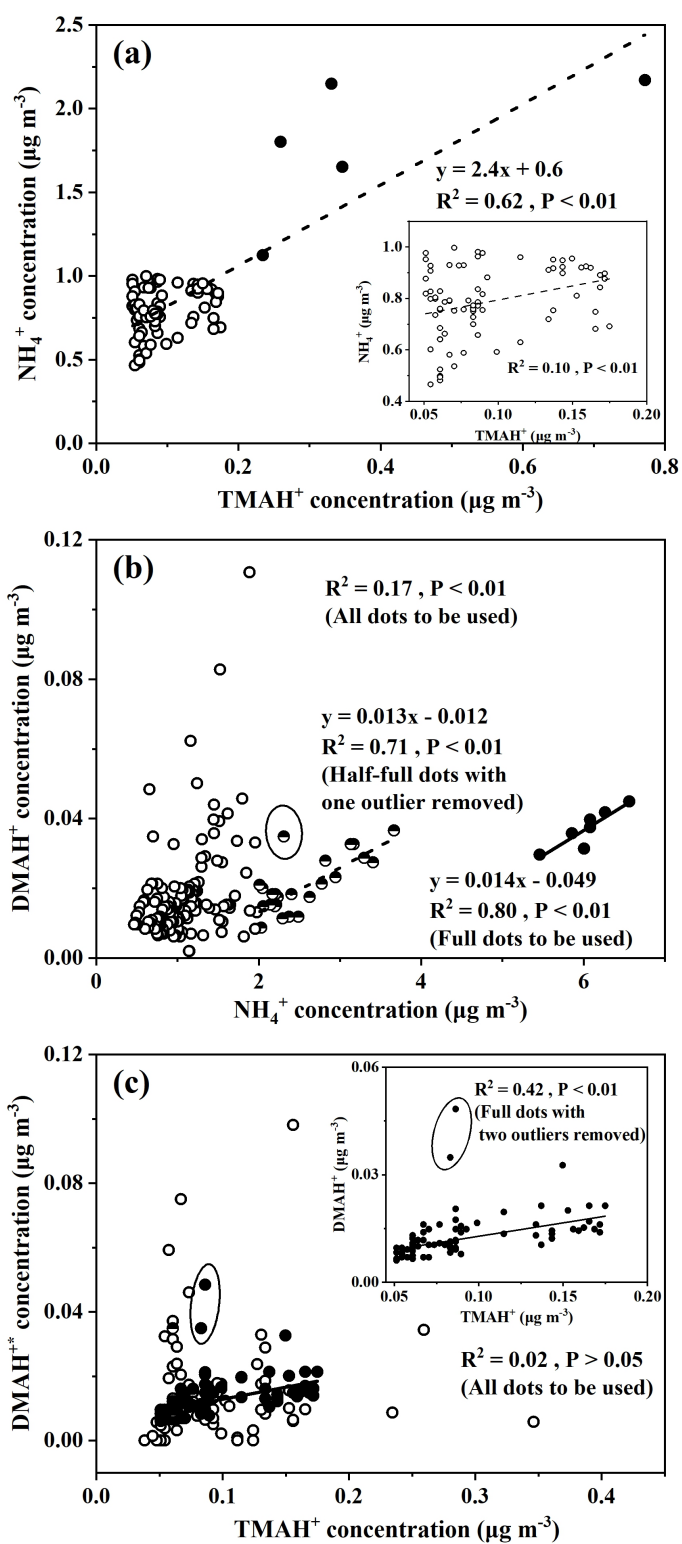
260

Figure 3: Correlations between concentrations of ions in PM2.5: (a) NH4+ versus TMAH+, and the samples when [NH4+]<1 µg m-3 in the inner frame; (b) DMAH+* versus NH4+; (c) DMAH+* versus TMAH+, and the samples when [NH4+]<1 µg m-3 in the inner frame. DMAH+* was defined in the text; full, half full, and

265 When the regression equation of [DMAH$^+$] = 0.013[NH$_4^+$] - 0.012, with the concentrations of NH$_4^+$ ranging from 1 μg m^{-3} to 2 μg m^{-3} as input, was used to estimate the concentrations of DMAH$^+$ from continental transport, the estimated concentrations accounted for 33±27% of the observed values. The sea-derived DMAH$^+$ in PM$_{2.5}$ was probably the major contributor to the observed values in most cases. In the outlier with a concentration of particulate NH$_4^+$ 2.3 μg m^{-3} (half full dot in Fig. 3b), the

270 contribution from continental transport was estimated to be 52%. When the concentrations of NH$_4^+$ were smaller than 1 μg m^{-3}, the values of continental DMAH$^+$ concentration predicted by the equation [DMAH$^+$] = 0.013[NH$_4^+$] - 0.012 were close to or smaller than zero. Thus, the observed DMAH$^+$ in PM$_{2.5}$, when NH$_4^+$ concentrations were below 1 μg m^{-3}, should be overwhelmed by marine sources. Under these conditions, a significant correlation with a low R^2 was

275 obtained between DMAH$^+$ and TMAH$^+$ when two outliers were removed (full dotes in Fig. 3c, R^2=0.42, P<0.01). Primary emissions of particulate DMAH$^+$ from the East China Sea likely contributed to the observed values to some extent. In four of the five episodic concentrations of particulate TMAH$^+$ ranging from 0.23 μg m^{-3} to 0.77 μg m^{-3}, the corresponding concentrations of particulate DMAH$^+$ varied from 0.011 μg m^{-3} to 0.018 μg m^{-3} and [DMAH$^+$]=0.011[TMAH$^+$]+0.011 (R^2=0.77). The

280 moderately good correlation supported the presence of primary particulate DMAH$^+$.

3.3 In-depth analysis during three episodes
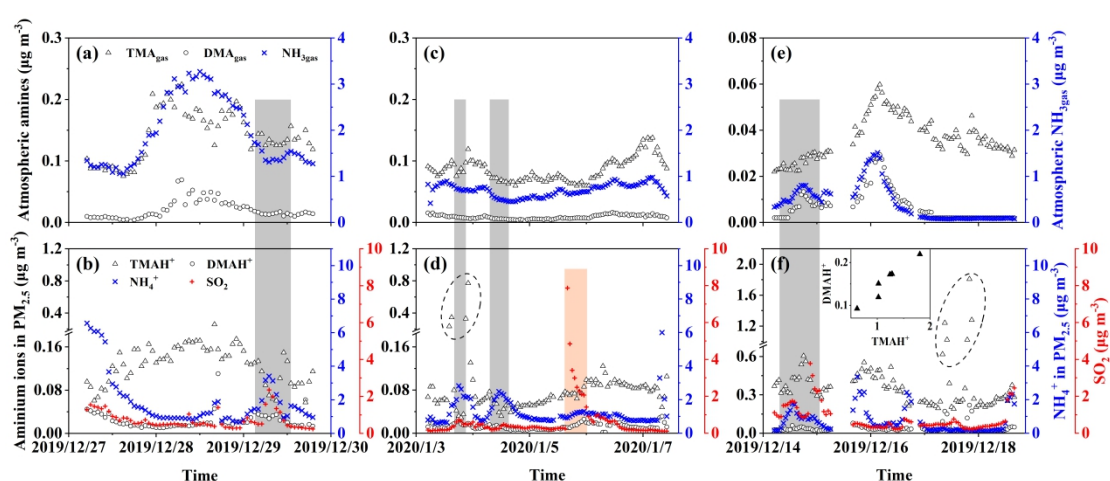
Figure 4: Times series of concentrations of gases and particulate ions during three episodes. Basic gases in E-period 1 (a); particulate ions and SO$_2$ in E-period 1 (b); (c) and (d) are the same as (a) and (b) except in

285 **E-period 2; (e) and (f) are the same as (a) and (b) except in E-period 3; gray and pink shadowing represent episodes with increasing NH_4^+ or SO_2, respectively; the figure superimposed in (f) shows the correlation between $TMAH^+$ and $DMAH^+$ in six cycling points in (f)**

Three episodes were further selected for deeper analyses of the sea-derived alkaline gases and primary particulate counterparts, during which continental transport was likely to have largely decreased.

290 E-period 1 started at 23:00LT on December 27 and ended at 13:00LT on December 30, 2019, when increases in concentrations of sea-derived gases and sea-derived primary $TMAH^+$ in $PM_{2.5}$ were observed over the East China Sea during Campaign B. E-period 2 also occurred in the East China Sea during Campaign B and started at 13:00LT on January 3 and ended at 18:00LT on January 7, 2020, when 1) an episodic increase in the sea-derived primary $TMAH^+$ in $PM_{2.5}$ occurred in the absence of a

295 corresponding increase in TMA_{gas}, and 2) an increase in the concentration of sea-derived TMA_{gas} was observed without a corresponding increase in sea-derived primary $TMAH^+$ present in $PM_{2.5}$. E-period 3 started at 00:00LT on 15 December and ended at 11:00LT on 19 December 2019 during Campaign A, when either an increase in the concentration of TMA_{gas} or particulate $TMAH^+$ was observed without a corresponding increase in their counterparts. The feature is similar to that of E-period 2.

300 Concentrations of $TMAH^+$ in $PM_{2.5}$ during E-periods 1 and 2 were smaller than those during period 3, and the reverse was generally true for concentrations of TMA_{gas}. The similar result can also be obtained from the observations over the East China Sea during Campaign B, in comparison with those measured during Campaign A. For example, the average concentration of $TMAH^+$ in $PM_{2.5}$ during Campaign A was 0.28 µg m^{-3} (Chen et al., 2021), approximately three times the corresponding average of 0.098 µg

305 m^{-3} during Campaign B.

Concentrations of TMA_{gas} and $TMAH^+$ in $PM_{2.5}$ were generally comparable during E-periods 1 and 2. However, concentrations of TMA_{gas} were approximately one order of magnitude smaller than those of $TMAH^+$ in $PM_{2.5}$ during E-period 3. A large difference between TMA_{gas} and particulate $TMAH^+$ was observed over the Yellow Sea and Bohai Sea throughout Campaign A. Several factors, for example,

310 surface seawater temperature, sea surface wind speed, and the concentration of $TMAH^+$ in surface seawater and/or the SML, may cause the disproportion, which are discussed as follows.

As we have analyzed, higher surface seawater temperatures, together with possibly higher concentrations of $TMAH^+$ in surface seawater, probably increased concentrations of TMA_{gas} over the

East China Sea, relative to those over the Yellow Sea and Bohai Sea. However, these two factors could not explain why concentrations of $TMAH^+$ in $PM_{2.5}$ over the East China Sea were lower than concentrations over the Yellow Sea and Bohai Sea. The release of sea spray aerosols is generally an exponential function of wind speed (Andreas, 1998; Leeuw et al., 2011; Feng et al., 2017). Thus, sea surface wind speeds were examined. Hourly average wind speeds were 7.3 ± 2.6 m s^{-1} over the East China Sea during Campaign B, which were not significantly different from those of 7.9 ± 8.1 m s^{-1} during Campaign A (P>0.05). Moreover, five hourly averages of $TMAH^+$ in $PM_{2.5}$ exceeded 1 µg m^{-3} over the Yellow Sea and Bohai Sea when wind speeds reached 12±0.5 m s^{-1}. During the nine hourly average wind speeds exceeding   12 m s^{-1} during the East China Sea cruise, the corresponding concentrations of $TMAH^+$ in $PM_{2.5}$ were only 0.08±0.01 µg m^{-3}. Five concentrations of $TMAH^+$ in $PM_{2.5}$ exceeded 0.2 µg m^{-3} in Campaign B, and wind speeds ranged from 5.6 to 8.1 m s^{-1} at those moments. Therefore, wind speeds alone could not explain why the observed concentrations of $TMAH^+$ in $PM_{2.5}$ over the East China Sea were lower than those over the Yellow Sea and the Bohai Sea.

Because the SML affects all mass transfers between the atmosphere and ocean (Cunliffe et al., 2013; Quinn, et al., 2015), the release of sea spray aerosols containing $TMAH^+$ should be affected by the abundance of $TMAH^+$ in SML, in addition to sea surface wind speeds and concentrations of $TMAH^+$ in bulk surface seawater. Combining the aforementioned observations, we argue that $TMAH^+$ may be more highly enriched in the SML than in bulk surface seawater over the Yellow Sea and the Bohai Sea during Campaign A under low surface seawater temperatures. Direct measurements of $TMAH^+$ enriched in the SML, as reported by van Pinxteren et al. (2019), are necessary to confirm this hypothesis.

During E-period 1, concentrations of TMA_{gas} and DMA_{gas} exhibited similar spatiotemporal patterns. Concentrations of NH_{3gas} exhibited a spatiotemporal pattern similar to that of gaseous amines during the initial period of increasing concentrations and the late period of decreasing concentrations, but not during the transition between early and late periods. Ratios of aminium to ammonium in bulk surface seawater and/or the SML of the corresponding sea zone may vary to some extent and complicate the observational results. Concentrations of particulate $TMAH^+$ exhibited a spatiotemporal pattern similar to that of gaseous amines, while a reverse spatiotemporal pattern was found for concentrations of particulate $DMAH^+$. Primary sea spray aerosols may contain substantially low concentrations of

particulate DMAH$^+$, as aforementioned. In addition, a significant decrease in the concentration of particulate TMAH$^+$ was apparent with increasing concentrations of particulate NH$_4^+$ and DMAH$^+$, as

345   well as those of SO$_2$ (gray shadowing in Fig. 4a). The unique decrease in particulate TMAH$^+$ also occurred in E-period 2 and E-period 3 (gray and pink shadowing in Fig. 4d, f), regardless of the simultaneous increase or decrease in concentrations of TMA$_{gas}$. Secondary chemical reactions probably converted particulate TMAH$^+$ to compounds undetectable by AIM-IC.

Unlike during E-period 1, the disproportional release of TMA$_{gas}$ with particulate TMAH$^+$ from the seas

350   probably occurred in E-periods 2 and 3. Moreover, a large increase in the concentration of particulate DMAH$^+$ was observed simultaneously with a large increase in particulate TMAH$^+$ in the six episodes observed over the Yellow Sea (Figure superimposed in Fig. 4f). However, only a small increase in particulate DMAH$^+$ was detected for the four episodes observed over the East China Sea (cycled empty triangles in Fig. 4d). This disproportion may also be ascribed to the spatiotemporal heterogeneity of the

355   enrichments of TMAH$^+$ and DMAH$^+$ in the SML.

3.4 Molar ratios of gaseous amines over NH$_{3gas}$ and their particulate counterparts

Dissociation constants (K_b) of TMA and DMA in water were 31 and 4 times that of NH$_3 \bullet$H$_2$O (Ge et al., 2011), respectively. Thus, DMA$_{gas}$ and TMA$_{gas}$ may enable the competitive neutralization of acids by NH$_{3gas}$ in the atmosphere (Almeida et al., 2013; Chen et al., 2016; Yao et al., 2018; Xie et al., 2018).

360   When the values of K_b were used to calculate effective Henry's Law constants for DMA (^{eff}KDMA), TMA (^{eff}KTMA), and NH$_3$ (^{eff}KNH$_3$), assuming the activity coefficients to be unity, the ratios of ^{eff}KDMA/^{eff}KNH$_3$ and ^{eff}KTMA/^{eff}KNH$_3$ were 16 and 0.6, respectively, at an ambient temperature of 298 K under acidic conditions (Ge et al., 2011). We considered the large differences between ^{eff}KDMA/^{eff}KNH$_3$ and ^{eff}KTMA/^{eff}KNH$_3$ and then separately examined the molar ratios of TMA$_{gas}$ to

365   NH$_{3gas}$ and the ratios of DMA$_{gas}$ to NH$_{3gas}$. Detailed equations are provided in Supporting Information.
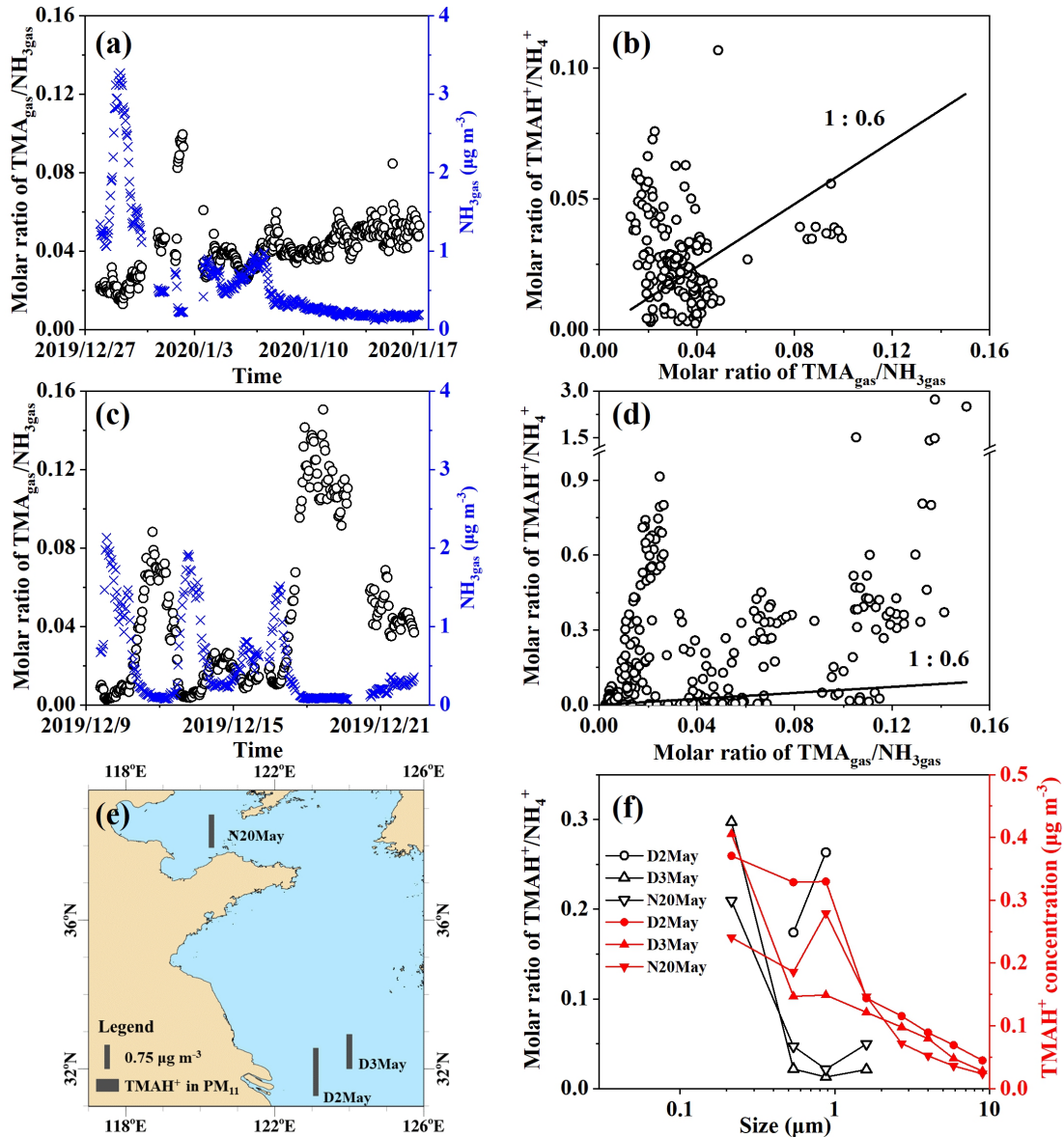
Figure 5: Time series of molar ratios of TMA_{gas}/NH_{3gas} (a) and (c) in Campaign B and A; correlation between TMA_{gas}/NH_{3gas} and $TMAH^+/NH_4^+$ (b) and (d) in Campaign B and A; map of particulate $TMAH^+$ (e) and size distributions of $TMAH^+/NH_4^+$ and mass concentrations of $TMAH^+$ (f) in Campaign C.

370   The ratios were first examined during Campaign B, when higher concentrations of TMA_{gas} and DMA_{gas} were observed than those observed during Campaign A. A large spatiotemporal variation in the molar ratio of TMA_{gas} to NH_{3gas}, ranging between 0.013 and 0.10 over the East China Sea, was observed from December 27, 2019 to January 7, 2020 (Fig. 5a). Low ratios of TMA_{gas} to NH_{3gas} with a mean of 0.022 ±0.004 occurred concurrently with higher concentrations of TMA_{gas} and NH_{3gas}, for example, from

375   23:00LT on December 27, 2019 to 13:00 LT on December 30, 2019 (Peak$_{TMA-1}$ in Fig. 1a). Increased

ratios of TMA_{gas} to NH_{3gas} of 0.08-0.10 occurred concurrently with the lowest concentrations of NH_{3gas}, ranging between 0.22 and 0.28 $\mu g\ m^{-3}$ from 22:00LT on 1 January to 07:00LT on 2 January 2020. This phenomenon may be related to the reuse of NH_4^+ by phytoplankton (Liu et al., 2013). In Campaign B over the Yellow Sea from 7 to 17 January 2020, the ratios exhibited a narrow range of 0.034 to 0.064;

380   one outlier of 0.085 was excluded (Fig. 5a).

During Campaign A over the Yellow Sea and Bohai Sea on 9-22 December, the molar ratios of TMA_{gas} to NH_{3gas} ranged from 0.003 to 0.15 (Fig. 5c). The ratios increased during the period from 17:00LT on December 17 to 16:00LT on December 19, with a mean of 0.12±0.014, because of a large decrease in the concentrations of NH_{3gas} (Figs. 5c and 4e). However, smaller ratios in the range of 0.011-0.016

385   were observed between 20:00LT on December 16 and 00:00LT on December 17 in the presence of the strong sea-derived emissions of alkaline gases (Figs. 5c and 4e). These results were consistent with those observed in Campaign B, indicating that the ratios of TMA_{gas} to NH_{3gas} during periods of episodic emission were likely decreased by half to one order of magnitude relative to those during periods of low emission.

390   The mean molar ratio of $TMAH^+$ to NH_4^+ in $PM_{2.5}$ was 0.032±0.019 during Campaign B over the East China Sea, comparable to those of TMA_{gas} to NH_{3gas} (Fig. 5c). When molar ratios of $TMAH^+$ to NH_4^+ in $PM_{2.5}$ were plotted against the ratios of TMA_{gas} to NH_{3gas}, data were scattered along the 1:0.6 line. However, no significant correlation was observed between them. The observed particulate $TMAH^+$ may co-exist externally with aerosols containing NH_4^+.

395   During Campaign A, the molar ratios of $TMAH^+$ to NH_4^+ largely varied with the 25th, 50th, 75th, and 90th percentile values of 0.009, 0.089, 0.35, and 0.56, respectively. As extremes, the 98th-100th percentile values ranged between 1.4 and 2.7 when concentrations of $TMAH^+$ in $PM_{2.5}$ exceeded 1 $\mu g\ m^{-3}$. When the molar ratios of $TMAH^+$ to NH_4^+ in $PM_{2.5}$ were plotted against the ratios of TMA_{gas} to NH_{3gas} (Fig. 5d), no significant correlation was apparent, and most of these data were distributed far

400   above the 1:0.6 line. Laboratory experiments are required to measure the thermodynamic gas-aerosol equilibria in the organic phase to explain these results (Pankow, 2015; Xie et al., 2018). Although the particulate TMA was detected as $TMAH^+$ by AIM-IC, it may not necessarily occur protonated in sea spray organic aerosols.

Measurements of ion concentrations in $PM_{2.5}$ do not demonstrate the size distributions of the ratios of

405    $TMAH^+$ to NH_4^+. Thus, three episodes, with concentrations of total particulate $TMAH^+$ exceeding 1 μg

m^{-3} in atmospheric particles with diameters smaller than 11 μm (PM_{11}) collected over the Yellow Sea

in 2012 (Hu et al., 2015), were included in the analysis. The sample collection sea zones are mapped in

Figure 5e. Size distributions of particulate $TMAH^+$ in the mass concentration and molar ratios of

$TMAH^+$ to NH_4^+ are shown in Figure 5f.

410   Concentrations of $TMAH^+$ generally increased from the bin-size of 7.0-11 μm to that of <0.43 μm (Fig.

1f), which were totally different from those of NH_4^+, which peaked at 0.65-1.1 μm (Figure was

superimposed in Fig. S1c). The unique size distributions of particulate $TMAH^+$ also implied that the

observed $TMAH^+$ was overwhelmingly derived from primary sea spray organic aerosols, based on

laboratory experimental results and field measurements (Ault et al., 2013; Prather et al., 2013; Hu et al.,

415   2015, 2018; Quinn et al., 2015). Notably, the mass concentration size distribution patterns of

particulate $TMAH^+$ were reported to be similar to those of NH_4^+ when secondary-formed particulate

$TMAH^+$ dominated the primary particulate $TMAH^+$ (Hu et al., 2018; Xie et al., 2018).

Ratios of $TMAH^+$ to NH_4^+ in bins of different sizes were also calculated. Assuming 1) gas-aerosol

equilibria were achieved and particulate $TMAH^+$ to NH_4^+ co-existed internally, ratios in different-sized

420   particles should theoretically approach a constant. However, ratios in particle size bins were distributed

across two ranges, namely, 0.2-0.3 and 0.01-0.05, corresponding to concentrations of NH_4^+ exceeding

0.9 μg m^{-3}, or below 0.6 μg m^{-3}, respectively, rejecting the null hypothesis. Notably, ratios were not

calculated in size bins when the concentrations of NH_4^+ were smaller than 0.1 μg m^{-3}. At such low

concentrations, analytic errors may be large and can be transferred to the calculated ratios.

425   Time series of ratios of DMA_{gas} to NH_{3gas}, particulate $DMAH^+$ to particulate NH_4^+, and their

correlations during Campaign A and B are shown in Figure S3a, b, c, d. Concentrations of $DMAH^+$ in

the three episodic samples collected in 2012 are mapped in Figure S3e. Size distributions of particulate

$DMAH^+$ in the mass concentration and molar ratios of $DMAH^+$ to NH_4^+ are shown in Figure S3f.

During Campaigns B and A, mean molar ratios of DMA_{gas} to NH_{3gas} were 0.004 ± 0.001 and

430   0.006±0.004, respectively. When molar ratios of $DMAH^+$ to NH_4^+ in $PM_{2.5}$ were plotted against ratios

of DMA_{gas} over NH_{3gas} (Fig. 5d), the data were far below the 1:16 line during Camping B. A possible

explanation is that sea-derived DMA_{gas} was not achieved with NH_4^+- containing aerosols from

continental transport. During Campaign A, most of the data were also far below the 1:16 line. However, a few points were close to or above the 1:16 line. The data were associated with the strong sea-derived primary particulate $DMAH^+$, which may co-exist externally with NH_4^+- containing aerosols. In addition, the size distributions of particulate $DMAH^+$ in the mass concentration and molar ratios of $DMAH^+$ to NH_4^+ in the three samples collected in 2012 were generally similar to those of $TMAH^+$. The analysis of particulate $TMAH^+$ was applied to that of particulate $DMAH^+$.

4 Conclusions and hypotheses

Semi-continuous measurements of the concentrations of basic gases and their counterparts over the East China Sea, Yellow Sea, and Bohai Sea showed large spatiotemporal variations. The average concentration of TMAgas was 0.10 ± 0.04 µg m^{-3} over the East China Sea in Campaign B, and decreased by approximately by 70% over the Yellow Sea and the Bohai Sea in Campaigns A and B, with the corresponding TMAgas concentration 0.031 ± 0.009 and 0.037 ± 0.011 µg m^{-3}. By contrast, the average concentration of $TMAH^+$ in $PM_{2.5}$ over the East China Sea was 0.098 ± 0.068 µg m^{-3}, and the average increased by approximately 200% to 0.28 ± 0.18 µg m^{-3} over the Yellow Sea and the Bohai Sea in Campaign A. Comprehensive analysis indicated that both TMA_{gas} and particulate TMAH+ were released from the seas. The disproportional release of TMA_{gas} and particulate $TMAH^+$ from the East China Sea, compared with that of the Yellow Sea and the Bohai Sea, however, indicated a differential enrichment of $TMAH^+$ in the SML.

In Campaign B, the average concentration of DMA_{gas} over the East China Sea was 0.012 ± 0.011 µg m^{-3}, and significantly decreased to 0.002 ± 0.001 µg m^{-3} over the Yellow Sea and the Bohai Sea. The moderately good correlation between DMA_{gas} and TMA_{gas} suggests that the observed DMA_{gas} was likely derived from marine emissions with TMA_{gas}. The average concentration of particulate $DMAH^+$ was 0.019 ± 0.014 µg m^{-3} over the East China Sea during Campaign B. When the concentration of NH_4^+ exceeded 2 µg m^{-3}, the corresponding particulate $DMAH^+$ was predominantly from long-range continental transport. However, the sea-derived $DMAH^+$ was probably the main contributor in most cases when the concentration of NH_4^+ was below 2 µg m^{-3}. When the concentration of NH_4^+ was below

We hypothesized that a lower surface seawater temperature would reduce the rate of biochemical degradation of polysaccharides, peptides, and protein gels (Carpenter et al., 2012; Prather et al., 2013; Quinn et al., 2015; Freedman, 2017) to small molecules in the Yellow Sea and Bohai Sea (Fig. 6). These compounds may highly accumulate in SML. Under higher surface seawater temperatures in the East China Sea, larger molecules may be largely decomposed into small molecules, TMA and DMA. TMA and DMA were dissolved in bulk seawater with less TMA and DMA enriched in the SML.

Based on the exponential correlation between basic gases and ambient temperature, we inferred that surface seawater temperature was probably one of the key factors controlling the release of TMA$_{gas}$, DMA$_{gas}$, and NH$_{3gas}$ from the seas to the atmosphere. Disproportional release of alkaline gases and corresponding particulate counterparts implied that enrichment of TMAH$^+$ and DMAH$^+$ in the SML may be overwhelmingly determined by the release of particulate TMAH$^+$ and DMAH$^+$, although the extent of enrichment may be largely affected by surface seawater temperature.
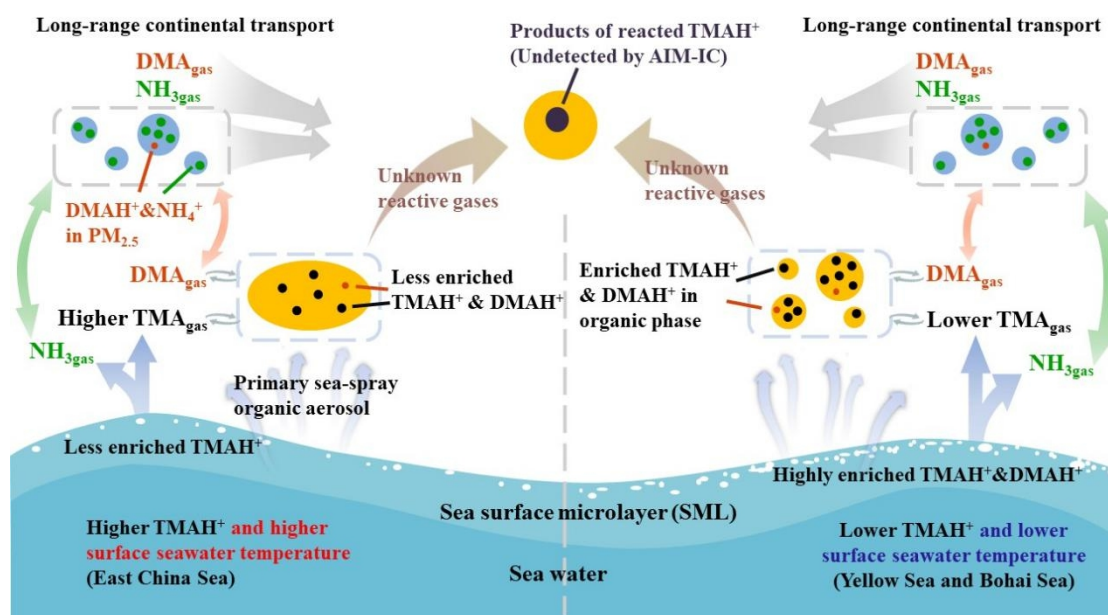
Figure 6: A schematic illustrating the release of basic gases and their counterparts from the two different seas and potential atmospheric reactions.

Combining no correlation between the molar ratios of TMAH$^+$ to NH$_4^+$ in PM$_{2.5}$, the ratios of TMA$_{gas}$ to NH$_{3gas}$, and the data with substantially larger ratios of TMAH$^+$ to NH$_4^+$ compared with those of

TMA$_{gas}$ to NH$_{3gas}$, we can infer that the observed TMAH$^+$ in the marine atmospheres was probably overwhelmed by primary sea spray organic aerosols and existed mainly in either the organic phase or

480   mixed phase. Secondary reactions in the marine atmosphere further led to the conversion of TMAH$^+$ into chemicals undetectable by AIM-IC, rather than forming new detectable particulate TMAH$^+$.

Sea-derived DMA$_{gas}$ and NH$_{3gas}$ were expected to exhibit an equilibrium with aerosols containing NH$_4^+$ and DMAH$^+$ from continental transport, but the equilibria were seemingly not achieved over the three seas. Thermodynamic models, including gas, aqueous phase, organic phase, and mixed phase, are

485   necessary to explain these results (Chan and Chan, 2013; Qiu and Zhang, 2013; Pankow, 2015; Chu and Chan, 2017; van Pinxteren et al., 2019).

Reuse of NH$_4^+$ by phytoplankton may also largely affect ratios of DMA$_{gas}$ to NH$_{3gas}$ and TMA$_{gas}$ to NH$_{3gas}$ in their emissions, which requires further investigation. The extent of degradation of TMA to DMA in different sea zones may vary significantly, leading to different ratios of DMAH$^+$ to TMAH$^+$ in

490   their primary marine emissions. These factors probably complicated the ratios of DMA$_{gas}$ to TMA$_{gas}$ and DMA$_{gas}$ (TMA$_{gas}$) to NH$_{3gas}$ in their marine emissions and should be considered when estimating their emissions.

In addition, primary particulate TMAH$^+$ and DMAH$^+$ were distributed mainly in submicron atmospheric particles. Their concentrations generally increased with decreasing particle size. By

495   contrast, the size distribution of secondary particulate DMAH$^+$ should be similar to that of particulate NH$_4^+$ (Xie et al., 2018; Hu et al., 2018). Considering the largely increased ratios of TMAH$^+$ to NH$_4^+$ in <0.43 µm particles, particles containing TMAH$^+$ may yield contributions comparable with anthropogenic particles to cloud condensation nuclei in less polluted marine atmospheres over the China Marginal Sea.

500   *Data availability.* The data of this paper are available upon request (contact: Xiaohong Yao, xhyao@ouc.edu.cn).

Acknowledgment

This research is supported by the National Key Research and Development Program in China (grant no. 2016YFC0200504), the Natural Science Foundation of China (grant no. 41776086)

505   **References**

Almeida, J., Schobesberger, S., Kürten, A., Ortega, I. K., Kupiainen-Määttä, O., Praplan, A. P., Adamov,

A., Amorim, A., Bianchi, F., Breitenlechner, M., David, A., Dommen, J., Donahue, N. M.,

Downard, A., Dunne, E., Duplissy, J., Ehrhart, S., Flagan, R. C., Franchin, A., Guida, R., Hakala, J.,

Hansel, A., Heinritzi, M., Henschel, H., Jokinen, T., Junninen, H., Kajos, M., Kangasluoma, J.,

510   Keskinen, H., Kupc, A., Kurtén, T., Kvashin, A. N., Laaksonen, A., Lehtipalo, K., Leiminger, M.,

Leppä, J., Loukonen, V., Makhmutov, V., Mathot, S., McGrath, M. J., Nieminen, T., Olenius, T.,

Onnela, A., Petäjä, T., Riccobono, F., Riipinen, I., Rissanen, M., Rondo, L., Ruuskanen, T., Santos,

F. D., Sarnela, N., Schallhart, S., Schnitzhofer, R., Seinfeld, J. H., Simon, M., Sipilä, M., Stozhkov,

Y., Stratmann, F., Tomé, A., Tröstl, J., Tsagkogeorgas, G., Vaattovaara, P., Viisanen, Y., Virtanen, A.,

515   Vrtala, A., Wagner, P. E., Weingartner, E., Wex, H., Williamson, C., Wimmer, D., Ye, P., Yli-Juuti,

T., Carslaw, K. S., Kulmala, M., Curtius, J., Baltensperger, U., Worsnop, D. R., Vehkamäki, H., and

Kirkby, J.: Molecular understanding of sulphuric acid–amine particle nucleation in the atmosphere,

Nature, 502, 359–363, https://doi.org/10.1038/nature12663, 2013.

Altieri, K. E., Hastings, M. G., Peters, A. J., Oleynik, S., and Sigman, D. M.: Isotopic evidence for a

520   marine ammonium source in rainwater at Bermuda, Global Biogeochem. Cycles, 28, 1066–1080,

https://doi.org/10.1002/2014GB004809, 2014.

Andreas, E. L.: A new sea spray generation function for wind speeds up to 32 m s-1, Journal of

figPhysical Oceanography, 28, 2175–2184,

https://doi.org/10.1175/1520-0485(1998)028<2175:ANSSGF>2.0.CO;2, 1998.

525   Ault, A. P., Moffet, R. C., Baltrusaitis, J., Collins, D. B., Ruppel, M. J., Cuadra-Rodriguez, L. A., Zhao,

D., Guasco, T. L., Ebben, C. J., Geiger, F. M., Bertram, T. H., Prather, K. A., and Grassian, V. H.:

Size-dependent changes in sea spray aerosol composition and properties with different seawater

conditions, Environmental Science & Technology, 47, 5603–5612,

https://doi.org/10.1021/es400416g, 2013.

530   Carpenter, L. J., Archer, S. D., and Beale, R.: Ocean-atmosphere trace gas exchange, Chem. Soc. Rev.,

41, 6473–6506, https://doi.org/10.1039/C2CS35121H, 2012.

Chan, L. P. and Chan, C. K.: Role of the Aerosol Phase State in Ammonia/Amines Exchange Reactions,

Environmental Science & Technology, 47, 5755–5762, https://doi.org/10.1021/es4004685, 2013.

Chen, H., Varner, M. E., Gerber, R. B., and Finlayson-Pitts, B. J.: Reactions of methanesulfonic acid

535  with amines and ammonia as a source of new particles in air, The Journal of Physical Chemistry B,

  120, 1526–1536, https://doi.org/10.1021/acs.jpcb.5b07433, 2016.

Chen, D., Shen, Y., Wang, J., Gao, Y., Gao, H., and Yao, X.: Semi-continuous observations of gaseous

  amines and ammonia and particulate counterparts in winter marine atmospheres over marginal seas

  of China: Identifying marine emission from continental transport (1), in preparation, 2021

540  Chu, Y. and Chan, C. K.: Reactive uptake of dimethylamine by ammonium sulfate and ammonium

  sulfate–sucrose mixed particles, The Journal of Physical Chemistry A, 121, 206–215,

  https://doi.org/10.1021/acs.jpca.6b10692, 2017.

Cunliffe, M., Engel, A., Frka, S., Gašparović, B., Guitart, C., Murrell, J. C., Salter, M., Stolle, C.,

  Upstill-Goddard, R., and Wurl, O.: Sea surface microlayers: A unified physicochemical and

545  biological perspective of the air–ocean interface, Progress in Oceanography, 109, 104–116,

  https://doi.org/10.1016/j.pocean.2012.08.004, 2013.

Dall'Osto, M., Airs, R. L., Beale, R., Cree, C., Fitzsimons, M. F., Beddows, D., Harrison, R. M.,

  Ceburnis, D., O'Dowd, C., Rinaldi, M., Paglione, M., Nenes, A., Decesari, S., and Simó, R.:

  Simultaneous detection of alkylamines in the surface ocean and atmosphere of the antarctic

550  sympagic environment, ACS Earth and Space Chemistry, 3, 854–862,

  https://doi.org/10.1021/acsearthspacechem.9b00028, 2019.

Deng, Y., Gao, T., Gao, H., Yao, X., and Xie, L.: Regional precipitation variability in East Asia related

  to climate and environmental factors during 1979-2012, Sci Rep, 4, 5693,

  https://doi.org/10.1038/srep05693, 2014.

555  Facchini, M. C., Decesari, S., Rinaldi, M., Carbone, C., Finessi, E., Mircea, M., Fuzzi, S., Moretti, F.,

  Tagliavini, E., Ceburnis, D., and O'Dowd, C. D.: Important source of marine secondary organic

  aerosol from biogenic amines, Environmental Science & Technology, 42, 9116–9121,

  https://doi.org/10.1021/es8018385, 2008.

Feng, L., Shen, H., Zhu, Y., Gao, H., and Yao, X.: Insight into generation and evolution of sea-salt

560  aerosols from field measurements in diversified marine and coastal atmospheres, Scientific Reports,

  7, 41260, https://doi.org/10.1038/srep41260, 2017.

Freedman, M. A.: Phase separation in organic aerosol, Chem. Soc. Rev., 46, 7694–7705, https://doi.org/10.1039/C6CS00783J, 2017.

Ge, X., Wexler, A. S., and Clegg, S. L.: Atmospheric amines – Part II. Thermodynamic properties and

565   gas/particle partitioning, Atmospheric Environment, 45, 561–577, https://doi.org/10.1016/j.atmosenv.2010.10.013, 2011.

Gibb, S. W., Mantoura, R. F. C., and Liss, P. S.: Ocean-atmosphere exchange and atmospheric speciation of ammonia and methylamines in the region of the NW Arabian Sea, Global Biogeochem. Cycles, 13, 161–178, https://doi.org/10.1029/98GB00743, 1999.

570   Hu, Q., Qu, K., Gao, H., Cui, Z., Gao, Y., and Yao, X.: Large increases in primary trimethylaminium and secondary dimethylaminium in atmospheric particles associated with cyclonic eddies in the northwest Pacific Ocean, Journal of Geophysical Research: Atmospheres, 123, 12133-12146, https://doi.org/10.1029/2018JD028836, 2018.

Hu, Q., Yu, P., Zhu, Y., Li, K., Gao, H., and Yao, X.: Concentration, size distribution, and formation of

575   trimethylaminium and dimethylaminium ions in atmospheric particles over marginal seas of China, Journal of the Atmospheric Sciences, 72, 3487–3498, https://doi.org/10.1175/JAS-D-14-0393.1, 2015.

Johnson, M., Sanders, R., Avgoustidi, V., Lucas, M., Brown, L., Hansell, D., Moore, M., Gibb, S., Liss, P., and Jickells, T.: Ammonium accumulation during a silicate-limited diatom bloom indicates the

580   potential for ammonia emission events, Marine Chemistry, 106, 63–75, https://doi.org/10.1016/j.marchem.2006.09.006, 2007.

Johnson, M. T., Liss, P. S., Bell, T. G., Lesworth, T. J., Baker, A. R., Hind, A. J., Jickells, T. D., Biswas, K. F., Woodward, E. M. S., and Gibb, S. W.: Field observations of the ocean-atmosphere exchange of ammonia: Fundamental importance of temperature as revealed by a comparison of high and low

585   latitudes, Global Biogeochem. Cycles, 22, GB1019, https://doi.org/10.1029/2007GB003039, 2008.

Köllner, F., Schneider, J., Willis, M. D., Klimach, T., Helleis, F., Bozem, H., Kunkel, D., Hoor, P., Burkart, J., Leaitch, W. R., Aliabadi, A. A., Abbatt, J. P. D., Herber, A. B., and Borrmann, S.: Particulate trimethylamine in the summertime Canadian high Arctic lower troposphere, Atmospheric Chemistry and Physics, 17, 13747–13766,

590   https://doi.org/10.5194/acp-17-13747-2017, 2017.

Leeuw, G. de, Andreas, E. L., Anguelova, M. D., Fairall, C. W., Lewis, E. R., O'Dowd, C., Schulz, M., and Schwartz, S. E.: Production flux of sea spray aerosol, Rev. Geophys., 49, RG2001, https://doi.org/10.1029/2010RG000349, 2011.

Lidbury, I., Murrell, J. C., and Chen, Y.: Trimethylamine N-oxide metabolism by abundant marine heterotrophic bacteria, Proceedings of the National Academy of Sciences, 111, 2710–2715, https://doi.org/10.1073/pnas.1317834111, 2014.

Lidbury, I. D., Murrell, J. C., and Chen, Y.: Trimethylamine and trimethylamine N-oxide are supplementary energy sources for a marine heterotrophic bacterium: implications for marine carbon and nitrogen cycling, The ISME Journal, 9, 760–769, https://doi.org/10.1038/ismej.2014.149, 2015.

Liu, Y., Zhang, T. R., Shi, J. H., Gao, H. W., and Yao, X. H.: Responses of chlorophyll a to added nutrients, Asian dust, and rainwater in an oligotrophic zone of the Yellow Sea: Implications for promotion and inhibition effects in an incubation experiment, J. Geophys. Res. Biogeosci., 118, 1763–1772, https://doi.org/10.1002/2013JG002329, 2013.

Lui, H.-K., Chen, C.-T. A., Lee, J., Wang, S.-L., Gong, G.-C., Bai, Y., and He, X.: Acidifying intermediate water accelerates the acidification of seawater on shelves: An example of the East China Sea, Continental Shelf Research, 111, 223–233, https://doi.org/10.1016/j.csr.2015.08.014, 2015.

Müller, C., Iinuma, Y., Karstensen, J., van Pinxteren, D., Lehmann, S., Gnauk, T., and Herrmann, H.: Seasonal variation of aliphatic amines in marine sub-micrometer particles at the Cape Verde islands, Atmospheric Chemistry and Physics, 9, 9587–9597, https://doi.org/10.5194/acp-9-9587-2009, 2009.

Pankow, J. F.: Phase considerations in the gas/particle partitioning of organic amines in the atmosphere, Atmospheric Environment, 122, 448–453, https://doi.org/10.1016/j.atmosenv.2015.09.056, 2015.

Paulot, F., Jacob, D. J., Johnson, M. T., Bell, T. G., Baker, A. R., Keene, W. C., Lima, I. D., Doney, S. C., and Stock, C. A.: Global oceanic emission of ammonia: Constraints from seawater and atmospheric observations, 29, 1165–1178, https://doi.org/10.1002/2015GB005106, 2015.

Perraud, V., Li, X., Jiang, J., Finlayson-Pitts, B. J., and Smith, J. N.: Size-resolved chemical composition of sub-20 nm particles from methanesulfonic acid reactions with methylamine and

620   ammonia, ACS Earth and Space Chemistry, 4, 1182–1194, https://doi.org/10.1021/acsearthspacechem.0c00120, 2020.

Prather, K. A., Bertram, T. H., Grassian, V. H., Deane, G. B., Stokes, M. D., Demott, P. J., Aluwihare, L. I., Palenik, B. P., Azam, F., Seinfeld, J. H., Moffet, R. C., Molina, M. J., Cappa, C. D., Geiger, F. M., Roberts, G. C., Russell, L. M., Ault, A. P., Baltrusaitis, J., Collins, D. B., Corrigan, C. E.,

625   Cuadra-Rodriguez, L. A., Ebben, C. J., Forestieri, S. D., Guasco, T. L., Hersey, S. P., Kim, M. J., Lambert, W. F., Modini, R. L., Mui, W., Pedler, B. E., Ruppel, M. J., Ryder, O. S., Schoepp, N. G., Sullivan, R. C., and Zhao, D.: Bringing the ocean into the laboratory to probe the chemical complexity of sea spray aerosol, Proc Natl Acad Sci U S A, 110, 7550–7555, https://doi.org/10.1073/pnas.1300262110, 2013.

630   Qiu, C. and Zhang, R.: Multiphase chemistry of atmospheric amines, Phys. Chem. Chem. Phys., 15, 5738–5752, https://doi.org/10.1039/C3CP43446J, 2013.

Quinn, P. K., Collins, D. B., Grassian, V. H., Prather, K. A., and Bates, T. S.: Chemistry and related properties of freshly emitted sea spray aerosol, Chemical Reviews, 115, 4383–4399, https://doi.org/10.1021/cr500713g, 2015.

635   Shao, Z., Shuai, L., Cheng, H., Wu, Z., You, F., Zhang, H., and Yao, J.: Influence of iron and carbon on the occurrence of Ulva prolifera (Ulvophyceae) in the Yellow Sea, Regional Studies in Marine Science, 36, 101224, https://doi.org/10.1016/j.rsma.2020.101224, available at: http://www.sciencedirect.com/science/article/pii/S2352485519303925, 2020.

van Neste, A., Duce, R. A., and Lee, C.: Methylamines in the marine atmosphere, Geophys. Res. Lett.,

640   14, 711–714, https://doi.org/10.1029/GL014i007p00711, 1987.

van Pinxteren, M., Fomba, K. W., van Pinxteren, D., Triesch, N., Hoffmann, E. H., Cree, C. H.L., Fitzsimons, M. F., Tümpling, W. von, and Herrmann, H.: Aliphatic amines at the Cape Verde Atmospheric Observatory: Abundance, origins and sea-air fluxes, Atmospheric Environment, 203, 183–195, https://doi.org/10.1016/j.atmosenv.2019.02.011, available at:

645   http://www.sciencedirect.com/science/article/pii/S1352231019301037, 2019.

Velthuis, M., van Deelen, E., van Donk, E., Zhang, P., and Bakker, E. S.: Impact of Temperature and Nutrients on Carbon: Nutrient Tissue Stoichiometry of Submerged Aquatic Plants: An Experiment and Meta-Analysis, Frontiers in Plant Science, 8, 655, https://doi.org/10.3389/fpls.2017.00655,

available at: https://www.frontiersin.org/article/10.3389/fpls.2017.00655, 2017.

650   Wentworth, G. R., Murphy, J. G., Croft, B., Martin, R., Pierce, J., Côté, J.-S., Courchesne, I., Tremblay,

J.-E., Gagnon, J., Thomas, J. L., Sharma, S., Toom, D., Chivulescu, A., Levasseur, M., and Abbatt,

J.: Ammonia in the summertime Arctic marine boundary layer: Sources, sinks, and implications,

Atmospheric Chemistry and Physics, 16, 1937–1953, https://doi.org/10.5194/acp-16-1937-2016,

2016.

655   Xie, H., Feng, L., Hu, Q., Zhu, Y., Gao, H., Gao, Y., and Yao, X.: Concentration and size distribution of

water-extracted dimethylaminium and trimethylaminium in atmospheric particles during nine

campaigns - Implications for sources, phase states and formation pathways, Science of The Total

Environment, 631-632, 130–141, https://doi.org/10.1016/j.scitotenv.2018.02.303, 2018.

Yao, X. and Zhang, L.: Analysis of passive-sampler monitored atmospheric ammonia at 74 sites across

660   southern Ontario, Canada, Biogeoscience, 10, 7913-7925, https://doi.org/10.5194/bg-10-7913-2013,

2013.

Yao, L., Garmash, O., Bianchi, F., Zheng, J., Yan, C., Kontkanen, J., Junninen, H., Mazon, S. B., Ehn,

M., Paasonen, P., Sipilä, M., Wang, M., Wang, X., Xiao, S., Chen, H., Lu, Y., Zhang, B., Wang, D.,

Fu, Q., Geng, F., Li, L., Wang, H., Qiao, L., Yang, X., Chen, J., Kerminen, V.-M., Petäjä, T.,

665   Worsnop, D. R., Kulmala, M., and Wang, L.: Atmospheric new particle formation from sulfuric

acid and amines in a Chinese megacity, Science, 361, 278–281,

https://doi.org/10.1126/science.aao4839, 2018.

Yu, F. and Luo, G.: Modeling of gaseous methylamines in the global atmosphere: impacts of oxidation

and aerosol uptake, Atmospheric Chemistry and Physics, 14, 12455–12464,

670   https://doi.org/10.5194/acp-14-12455-2014, 2014.

Zhang, C., Ito, A., Shi, Z., Aita, M. N., Yao, X., Chu, Q., Shi, J., Gong, X., and Gao, H.: Fertilization of

the northwest Pacific Ocean by East Asia air pollutants, Global Biogeochem. Cycles, 33, 690–702,

https://doi.org/10.1029/2018GB006146, 2019a.

Zhang, C., Yao, X., Chen, Y., Chu, Q., Yu, Y., Shi, J., and Gao, H.: Variations in the phytoplankton

675   community due to dust additions in eutrophication, LNLC and HNLC oceanic zones, Science of

The Total Environment, 669, 282–293, https://doi.org/10.1016/j.scitotenv.2019.02.068, 2019b.

Zheng, J., Ma, Y., Chen, M., Zhang, Q., Wang, L., Khalizov, A. F., Yao, L., Wang, Z., Wang, X., Chen, L.: Measurement of atmospheric amines and ammonia using the high resolution time-of-flight chemical ionization mass spectrometry, Atmospheric Environment, 102, 249-259, http://doi.org/10.1016/j.atmosenv.2014.12.002, 2015.

Zhou, S., Li, H., Yang, T., Chen, Y., Deng, C., Gao, Y., Chen, C., and Xu, J.: Characteristics and sources of aerosol aminiums over the eastern coast of China: Insights from the integrated observations in a coastal city, adjacent island and surrounding marginal seas, Atmospheric Chemistry and Physics, 19, 10447–10467, https://doi.org/10.5194/acp-19-10447-2019, 2019.

Zhu, Y., Li, K., Shen, Y., Gao, Y., Liu, X., Yu, Y., Gao, H., and Yao, X.: New particle formation in the marine atmosphere during seven cruise campaigns, Atmospheric Chemistry and Physics, 19, 89–113, https://doi.org/10.5194/acp-19-89-2019, 2019.